

Complete photonic bandgaps in supercell photonic crystals

Alexander Cerjan and Shanhui Fan

*Department of Electrical Engineering, and Ginzton Laboratory,
Stanford University, Stanford, California 94305, USA*

(Dated: April 28, 2017)

We develop a class of supercell photonic crystals supporting complete photonic bandgaps based on breaking spatial symmetries of the underlying primitive photonic crystal. One member of this class based on a two-dimensional honeycomb structure supports a complete bandgap for an index-contrast ratio as low as $n_{high}/n_{low} = 2.1$, making this the first such 2D photonic crystal to support a complete bandgap in lossless materials at visible frequencies. The complete bandgaps found in such supercell photonic crystals do *not* necessarily monotonically increase as the index-contrast in the system is increased, disproving a long-held conjecture of complete bandgaps in photonic crystals.

Since their discovery, photonic crystals have become an indispensable technology across the entire field of optical physics due to their ability to confine and control light of an arbitrary wavelength [1–4]. This critical feature is achieved by designing the crystal lattice to possess a complete photonic bandgap, a range of frequencies for which no light can propagate regardless of its momentum or polarization. Unlike their electronic counterparts in conventional crystals, whose band structure is limited to the crystal lattices available in atomic and molecular structures, the dielectric structure comprising a photonic crystal can be specified with nearly complete arbitrariness, yielding a vast design space for optimizing photonic crystals for specific applications that is limited only by the index of refraction of available materials at the operational wavelength. For example, photonic crystals have been developed to promote absorption in monolayer materials [5, 6], or for use in achieving high-power solid-state lasers [7–9]. Moreover, this design freedom in dielectric structures has been leveraged in numerous studies to optimize the complete bandgaps in high-index materials [10–31]. Unfortunately, similar efforts to realize new crystal structures or improve upon existing ones to achieve complete bandgaps in low-index materials have yielded only minor improvements upon traditional simple crystal structures with high symmetry [32, 33], i.e. the inverse triangular lattice in two-dimensions [4] and the network diamond lattice in three-dimensions [34]. This has led many to conclude that the known high-symmetry dielectric structures are nearly optimal for achieving low-index complete bandgaps [33].

However, the ability to realize complete bandgaps for low-index materials is critically important to the development of many photonics technologies operating in the visible wavelength range, such as augmented and virtual reality systems, where the highest index lossless materials have $n \approx 2.4$ – 2.5 . Currently, there are no known 2D photonic crystals which display a complete bandgap in this index contrast regime, and thus it is not possible to realize dual-polarization in-plane guiding at this index contrast using photonic crystal slabs. Although a few 3D photonic crystals do display a complete bandgap in

this range, 3D photonic crystals are difficult to fabricate [35–39].

In this Letter, we demonstrate a new class of complete photonic bandgaps which are achieved by judiciously breaking symmetry, rather than promoting it. By starting with a photonic crystal possessing a large bandgap for one polarization, we show that by expanding the primitive cell of the photonic crystal to form a supercell and then slightly adjusting the dielectric structure within this supercell to break part of the translational symmetry of the original primitive cell, a bandgap in the other polarization can be opened, thus producing a complete bandgap. This method yields a two-dimensional photonic crystal based on a honeycomb lattice with a complete bandgap that persists down to an index-contrast ratio of $n_{high}/n_{low} = 2.1$, the lowest known index-contrast ratio in 2D photonic crystals. Such low index contrast bandgaps can also be translated into photonic crystal slabs, where they represent the first structures able to confine optical frequencies in-plane regardless of their polarization. In contrast to the complete photonic bandgaps found in traditional photonic crystals, complete bandgaps in supercell photonic crystals do not necessarily monotonically increase as a function of the index-contrast ratio, disproving a long-held conjecture in the photonic crystal literature [4].

To illuminate how symmetry breaking can help to realize complete photonic bandgaps, we first consider the 2D photonic crystal comprised of a network structure on a honeycomb lattice depicted in Fig. 1(a). The primitive cell of this system contains a pair of vertices in this network lattice, and the system can be parameterized solely in terms of the thickness, t , of the lines forming the network structure. Although in a low-index network structure, $n_{high}/n_{low} = 2.4$, a wide range of t yields a large transverse electric (TE) bandgap as shown in Fig. 1(b), no complete photonic bandgap exists for any choice of t for this choice of n_{high}/n_{low} .

However, starting from the crystal structure as shown in Fig. 1(a), we can find a complete bandgap in a closely related supercell photonic crystal. First, we increase the size of the primitive cell to contain six vertices which

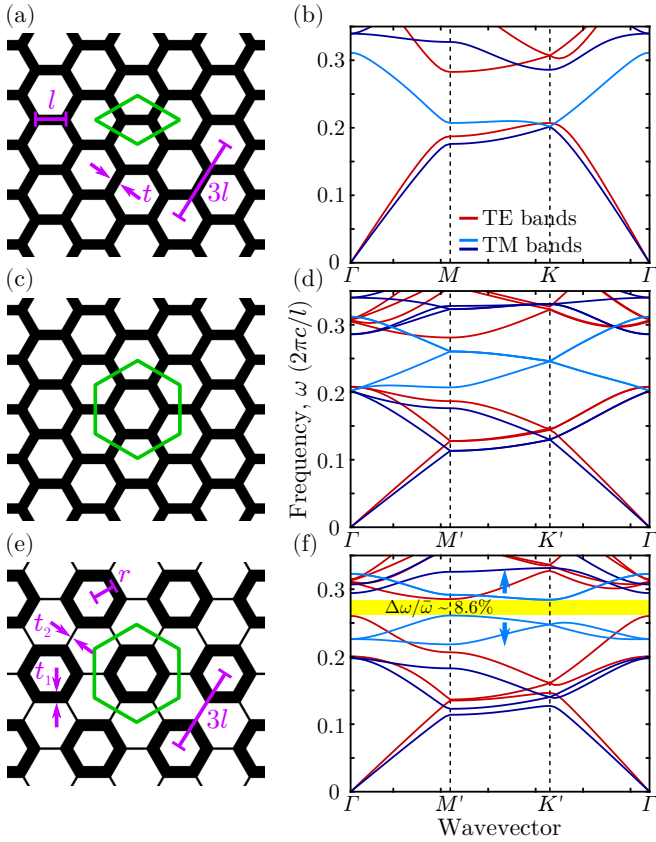


FIG. 1. (a),(c),(e) Schematics of 2D photonic crystals formed of a network of a high dielectric material with $n = 2.4$ (black region) in a background of air, $n_{\text{air}} = 1$. The unit cell for the corresponding band structure in (b),(d),(f) is shown in green. Parameters which characterize these crystals are indicated in purple. The structures in (a) and (c) are completely specified by the line thickness, t , while the structure in (e) is completely specified by three parameters, the thick line thickness, t_1 , the thin line thickness, t_2 , and the shortest distance from a thick line to the center of its corresponding thick-bordered hexagon, r . l denotes the distance between two vertices in the primitive honeycomb lattice. (b),(d),(f) Band structures around the border of the irreducible Brillouin Zone for the photonic crystals shown in (a),(c),(e), respectively, in which the TE bands are shown in red and the TM bands are shown in blue. In (b), the 2nd TM band is shown as cyan, while the corresponding folded bands in the supercell Brillouin zone in (d) and (f) are also shown in cyan. In (b),(d), $t/l = 0.3636$, while in (f), $t_1/l = 0.4149$, $t_2/l = 0.0816$, and $r/l = 0.8145$, and a complete bandgap is found with width $\Delta\omega/\omega_0 = 8.6\%$ between the 8th and 9th bands, shown in yellow. Band structures were calculated using MIT PHOTONIC BANDS (MPB) [40].

form the supercell, as depicted in Fig. 1(c). In doing so, each of the bands in the primitive Brillouin zone fold up into three bands in the supercell Brillouin zone, shown in Fig. 1(d). Along the edge of the supercell Brillouin zone ($M' \rightarrow K'$), pairs of the folded supercell bands can form lines of degeneracies, i.e. degenerate contours [41], and one such degenerate contour is formed per trio of

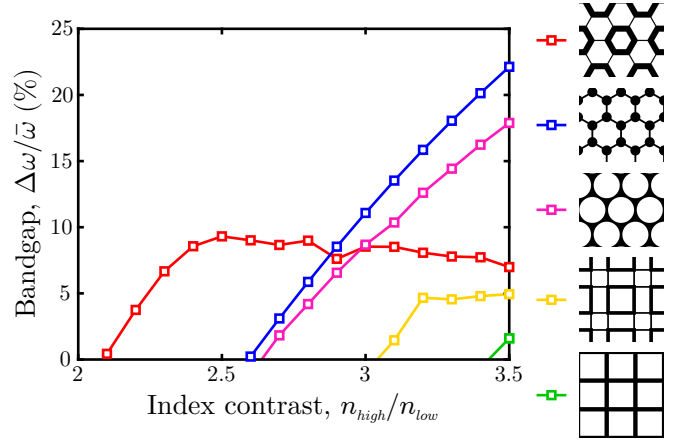


FIG. 2. Plot of the optimized complete bandgap width as a function of the index contrast, $n_{\text{high}}/n_{\text{low}}$ for five different 2D photonic crystals, supercell network honeycomb lattice discussed in Fig. 1 (red), traditional inverse triangular lattice discussed in Ref. [32] (blue), traditional network square lattice (green), and supercell network square lattice discussed in Fig. 4 (yellow). The black regions correspond to the high index material, n_{high} , while the white regions correspond to low index material, n_{low} . Optimized complete bandgaps were calculated using MPB [40].

folded bands originating from the same band in the primitive Brillouin zone. From the perspective of the supercell photonic crystal, the degeneracies comprising each of the degenerate contours are accidental, and are only the result of the supercell obeying an extra set of spatial symmetries as it is a three-fold copy of the original photonic crystal. Thus by breaking these symmetries, the degeneracies forming the degenerate contours are lifted, and a gap can begin to open between the two transverse magnetic (TM) bands. The supercell is now characterized in terms of three parameters, the thickness of the center lines, t_1 , the thickness of the connecting lines, t_2 , and the size of the thick-lined hexagons, r , shown in Fig. 1(e). When the symmetry breaking becomes sufficiently strong, a complete photonic bandgap opens between the 8th and 9th bands of the system, whose maximum width at $n_{\text{high}}/n_{\text{low}} = 2.4$ can be found numerically to be $\Delta\omega/\bar{\omega} = 8.6\%$. Here, $\Delta\omega$ is the difference between the minimum of the 9th band and the maximum of the 8th band, while $\bar{\omega}$ is the central frequency between the two bands. Rigorously, after the symmetry of this system is broken, the supercell containing six vertices becomes the primitive cell of the system. However, for semantic convenience, we will continue to refer to this larger primitive cell as the ‘supercell’ and reserve ‘primitive cell’ for the smaller system whose symmetry is intact.

Previously, the lowest index-contrast ratio known to support a complete bandgap in a 2D photonic crystal was a decorated honeycomb lattice, shown as the blue curve in Fig. 2, which has a complete bandgap between

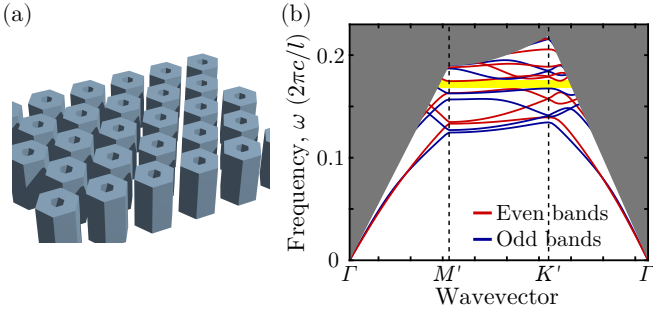


FIG. 3. (a) Schematics of a 3D photonic crystal slab consisting of high dielectric hexagonal rods with $n = 2.4$ in a background of air, $n_{\text{air}} = 1$, each of which also contains a hexagonal air hole in its center. This system can be completely parameterized using exactly the same choice of t_1 , t_2 , and r from the 2D photonic crystal shown in Fig. 1(e), as well as the height of each rod, h . For the structure in (a) $t_2 = 0$. (b) Band diagram for the photonic crystal slab shown in (a), in which the even modes with respect to the mirror plane at $z = 0$ are shown in red, while the odd modes are shown in blue. The grey regions of the band diagram indicate the continuum of radiation modes which lies above the light line. As can be seen, a complete bandgap with width $\Delta\omega/\omega_0 = 4.3\%$ (yellow) opens between the 7th and 8th bands for $t_1/l = 0.7482$, $t_2/l = 0$, $r/l = 0.7405$, and $h/l = 3.564$, where l is again the distance between two vertices in the underlying primitive honeycomb lattice. Band structures were calculated using MPB [40].

the 3rd and 4th bands for index-contrast ratios as low as $n_{\text{high}}/n_{\text{low}} = 2.6$ [32]. This structure provides a relatively modest improvement upon the traditional triangular lattice of air holes, also shown in Fig. 2 as the pink curve. In contrast, the supercell honeycomb lattice possesses a complete bandgap for index-contrast ratios as low as $n_{\text{high}}/n_{\text{low}} = 2.1$, and as such is the first 2D photonic crystal design that can realize a complete bandgap for visible wavelengths where the largest index of refraction possible in lossless materials is $n \approx 2.4$ – 2.5 , which is found in Diamond [42], Titanium Dioxide [43], and Strontium Titanate [44]. Furthermore, this supercell honeycomb structure could also be used in conjunction with high-index materials available in other frequency ranges so that the low-index material used in the structure need not be air. For example, this could enable realizing complete bandgaps in completely solid photonic crystal fibers operating in the communications band, where the high index regions are Silicon, $n_{\text{high}} = 3.48$, and the low-index regions are filled with fused silica, $n_{\text{low}} = 1.45$, such that $n_{\text{high}}/n_{\text{low}} = 2.4$ for $\lambda = 1.55\mu\text{m}$.

This 2D supercell honeycomb structure can also be used to design new photonic crystal slabs so as to provide confinement in three dimensions. In Fig. 3, we show a supercell honeycomb slab with a complete below-light-line dual-polarization bandgap of $\Delta\omega/\omega_0 = 4.3\%$ for $n_{\text{high}}/n_{\text{low}} = 2.4$. Note that in photonic crystal slabs, to define a band gap one only considers the phase space re-

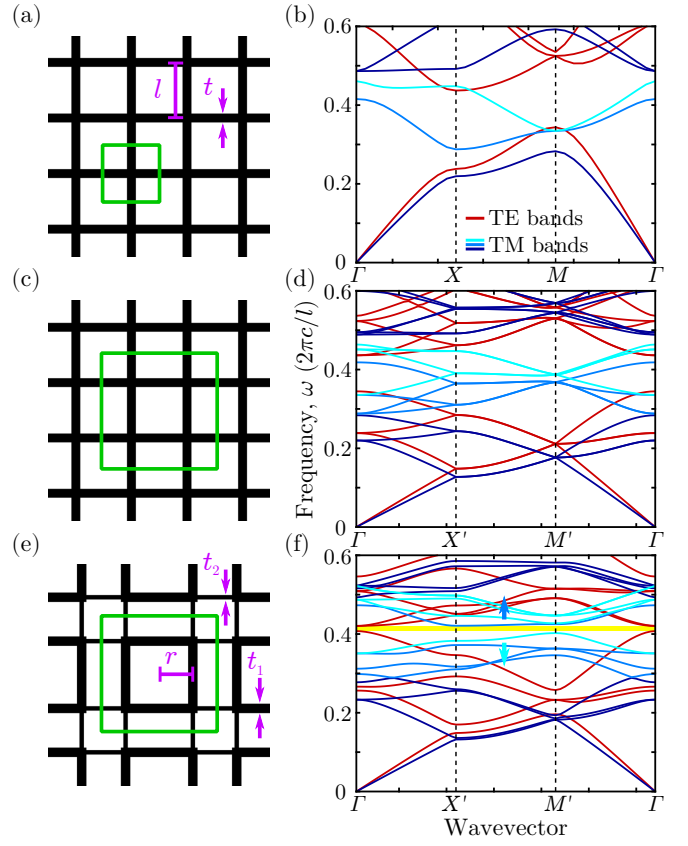


FIG. 4. (a),(c),(e) Schematics of 2D photonic crystals formed of a network of a high dielectric material with $n = 3.2$ (black region) in a background of air, $n_{\text{air}} = 1$. The unit cell for the corresponding band structure in (b),(d),(f) is shown in green. Parameters which characterize these crystals are indicated in purple. The structures in (a) and (c) are completely specified by the line thickness, t , while the structure in (e) is completely specified by three parameters, the thick-line thickness, t_1 , the thin-line thickness, t_2 , and the shortest distance from a thick line to the center of its corresponding thick-line bordered square, r . l denotes the distance between two vertices in the primitive cell. (b),(d),(f) Band structures around the border of the irreducible Brillouin Zone for the photonic crystals shown in (a),(c),(e), respectively, in which the TE bands are shown in red and the TM bands are shown in blue. In (b), the 2nd (3rd) TM band is shown as light blue (cyan), while the corresponding folded bands in the supercell Brillouin zone in (d) and (f) are also shown in light blue (cyan). In (b),(d), $t/a_{\text{PC}} = 0.32$, while in (f), $t_1/a_{\text{PC}} = 0.34$, $t_2/a_{\text{PC}} = 0.16$, and $r/a_{\text{PC}} = 0.605$, and a complete bandgap is found with width $\Delta\omega/\omega_0 = 4.6\%$ between the 12th and 13th bands, shown in yellow. Band structures were calculated using MPB [40].

gions below the light line, as above the light line the radiation modes form a continuum with no gaps. To the best of our knowledge, this represents the first system which could confine visible frequencies emitted from an omnipolarization source buried within the system. Likewise, this design could also be used to realize entirely solid photonic crystal slabs for communications frequencies where

higher index dielectric materials are available.

The procedure used above is not restricted to the honeycomb lattice. To illustrate this point, we use the same method to produce a complete bandgap in a 2D supercell square network lattice, as shown in Fig. 4. Unlike in the primitive honeycomb crystal, the TE bandgap in the underlying primitive square lattice is spanned by two TM bands. Thus, a complete bandgap is only realized for sufficiently strong symmetry breaking so that not only does a gap open in each degenerate contour of the folded supercell TM bands, but that a gap opens between these two folded bands. This limits the overall width of the complete bandgap, and the lowest index-contrast ratio for which this structure possesses a complete bandgap is $n_{high}/n_{low} \sim 3.1$, as shown as the yellow line in Fig. 2. However, this still represents a significant improvement upon the range of index-contrast ratios which can yield a complete bandgap when compared against other 2D photonic crystals based on a square lattice.

Complete bandgaps in supercell photonic crystal possess three features which distinguish them from complete bandgaps found in traditional photonic crystals. First, as noted above, these structures have been designed by specifically breaking symmetry within the system. This is entirely distinct from what is observed for bandgaps found in traditionally designed structures, which consider the high-symmetry triangular lattice in 2D and diamond lattice in 3D to be near optimal. Second, as can be seen in Fig. 2, complete bandgaps in supercell structures do not necessarily monotonically increase in size as a function of the index-contrast. This disproves a long-held conjecture of complete bandgaps in photonic crystals, that the optimized bandgap (between the same two bands) always increases as the index contrast increases [4]. Finally, the complete bandgap in supercell crystals is found between higher order bands. This is unlike many photonic crystal structures previously considered where the complete bandgap occurs between lower-order bands.

Designing two-dimensional supercell photonic crystals to possess complete bandgaps has three steps. First, a candidate primitive photonic crystal must be constructed which possesses a large bandgap for one polarization, and which is spanned by at most one or two bands in the other polarization. Second, a supercell must be generated from this primitive cell such that the degenerate contours of the folded band spanning the single-polarization bandgap lie entirely within the single-polarization bandgap. Finally, the supercell perturbation which breaks the underlying primitive cell symmetries must be designed, such that a bandgap in the degenerate contour opens before the single-polarization bandgap in the original primitive system closes.

We expect these same design principles to hold for finding complete bandgaps in three-dimensional supercell photonic crystals, but in practice we have been unable to find such a structure. Although the second and

third steps in the above procedure are relatively straightforward, finding good candidate primitive cell structures is much more challenging in 3D, as it is rare to find what would be a large bandgap spanned by only a single other band. For comparison, this is relatively easy in 2D, structures with isolated dielectric elements typically possess large TM bandgaps, but not TE bandgaps, while network structures typically possess large TE bandgaps, but no TM bandgaps.

In conclusion, we have developed a new class of photonic crystals which support complete bandgaps which stem from breaking spatial symmetries. These structures can exhibit complete bandgaps for much lower index-contrast ratios than was previously known, enabling the confinement of visible light in two-dimensional structures. The discovery of this new class of supercell structures also provides encouragement that there may be significant improvements remaining to be discovered in designing and optimizing complete bandgaps at low index-contrasts in both two- and three-dimensional systems.

This work was supported by an AFOSR MURI program (Grant No. FA9550-12-1-0471), and an AFOSR project (Grant No. FA9550-16-1-0010).

-
- [1] E. Yablonovitch, Phys. Rev. Lett. **58**, 2059 (1987).
 - [2] S. John, Phys. Rev. Lett. **58**, 2486 (1987).
 - [3] J. D. Joannopoulos, P. R. Villeneuve, and S. Fan, Nature **386**, 143 (1997).
 - [4] J. D. Joannopoulos, S. G. Johnson, J. N. Winn, and R. D. Meade, *Photonic Crystals: Molding the Flow of Light (Second Edition)* (Princeton University Press, 2011).
 - [5] J. R. Piper and S. Fan, ACS Photonics **1**, 347 (2014).
 - [6] J. R. Piper, V. Liu, and S. Fan, Appl. Phys. Lett. **104**, 251110 (2014).
 - [7] S. Noda, M. Yokoyama, M. Imada, A. Chutinan, and M. Mochizuki, Science **293**, 1123 (2001).
 - [8] Y. Kurosaka, S. Iwahashi, Y. Liang, K. Sakai, E. Miyai, W. Kunishi, D. Ohnishi, and S. Noda, Nat Photon **4**, 447 (2010).
 - [9] K. Hirose, Y. Liang, Y. Kurosaka, A. Watanabe, T. Sugiyama, and S. Noda, Nat Photon **8**, 406 (2014).
 - [10] S. Fan, P. R. Villeneuve, R. D. Meade, and J. D. Joannopoulos, Appl. Phys. Lett. **65**, 1466 (1994).
 - [11] D. Dobson and S. Cox, SIAM J. Appl. Math. **59**, 2108 (1999).
 - [12] M. Doosje, B. J. Hoenders, and J. Knoester, J. Opt. Soc. Am. B **17**, 600 (2000).
 - [13] S. J. Cox and C. Dobson, J. Comput. Phys. **158**, 214 (2000).
 - [14] S. G. Johnson and J. D. Joannopoulos, Appl. Phys. Lett. **77**, 3490 (2000).
 - [15] L. Shen, S. He, and S. Xiao, Phys. Rev. B **66**, 165315 (2002).
 - [16] R. Biswas, M. Sigalas, K. Ho, and S. Lin, Phys. Rev. B **65**, 205121 (2002).
 - [17] M. Maldovan, A. Urbas, N. Yufa, W. Carter, and

- E. Thomas, Phys. Rev. B **65**, 165123 (2002).
- [18] M. Maldovan, C. K. Ullal, W. C. Carter, and E. L. Thomas, Nat Mater **2**, 664 (2003).
- [19] K. Michielsen and J. S. Kole, Phys. Rev. B **68**, 115107 (2003).
- [20] O. Sigmund and J. S. Jensen, Philos. Trans. R. Soc. A **361**, 1001 (2003).
- [21] O. Toader, M. Berciu, and S. John, Phys. Rev. Lett. **90**, 233901 (2003).
- [22] J. S. Jensen and O. Sigmund, Appl. Phys. Lett. **84**, 2022 (2004).
- [23] M. B. Stanley, S. J. Osher, and E. Yablonovitch, IEICE Trans. Electron. **87**, 258 (2004).
- [24] C. Y. Kao, S. Osher, and E. Yablonovitch, Appl. Phys. B **81**, 235 (2005).
- [25] M. Maldovan and E. L. Thomas, J. Opt. Soc. Am. B **22**, 466 (2005).
- [26] S. Halkjær, O. Sigmund, and J. S. Jensen, Struct. Multidiscip. Optim. **32**, 263 (2006).
- [27] Y. Watanabe, Y. Sugimoto, N. Ikeda, N. Ozaki, A. Mizutani, Y. Takata, Y. Kitagawa, and K. Asakawa, Opt. Express **14**, 9502 (2006).
- [28] O. Sigmund and K. Hougaard, Phys. Rev. Lett. **100**, 153904 (2008).
- [29] H. Men, N. C. Nguyen, R. M. Freund, P. A. Parrilo, and J. Peraire, Journal of Computational Physics **229**, 3706 (2010).
- [30] L. Jia and E. L. Thomas, Phys. Rev. A **84**, 033810 (2011).
- [31] X. Liang and S. G. Johnson, Opt. Express **21**, 30812 (2013).
- [32] A. F. Oskooi, J. D. Joannopoulos, and S. G. Johnson, Opt. Express **17**, 10082 (2009).
- [33] H. Men, K. Y. K. Lee, R. M. Freund, J. Peraire, and S. G. Johnson, Opt. Express **22**, 22632 (2014).
- [34] M. Maldovan and E. L. Thomas, Nat Mater **3**, 593 (2004).
- [35] E. Yablonovitch, J. Opt. Soc. Am. B **10**, 283 (1993).
- [36] S. Y. Lin, J. G. Fleming, D. L. Hetherington, B. K. Smith, R. Biswas, K. M. Ho, M. M. Sigalas, W. Zubrzycki, S. R. Kurtz, and J. Bur, Nature **394**, 251 (1998).
- [37] S. Noda, K. Tomoda, N. Yamamoto, and A. Chutinan, Science **289**, 604 (2000).
- [38] Y. A. Vlasov, X.-Z. Bo, J. C. Sturm, and D. J. Norris, Nature **414**, 289 (2001).
- [39] M. Qi, E. Lidorikis, P. T. Rakich, S. G. Johnson, J. D. Joannopoulos, E. P. Ippen, and H. I. Smith, Nature **429**, 538 (2004).
- [40] S. G. Johnson and J. D. Joannopoulos, Opt. Express **8**, 173 (2001).
- [41] A. Cerjan, A. Raman, and S. Fan, Phys. Rev. Lett. **116**, 203902 (2016).
- [42] H. R. Phillip and E. A. Taft, Phys. Rev. **136**, A1445 (1964).
- [43] J. R. DeVore, J. Opt. Soc. Am. **41**, 416 (1951).
- [44] M. J. Weber, *CRC Handbook of Laser Science and Technology Supplement 2: Optical Materials* (CRC Press, 1994).